Submitted to the
XXXIst International Conference on High Energy Physics
24–31 July 2002, Amsterdam, The Netherlands

Abstract: 906 **Parallel Session: 10**

Search for lepton-flavor violation in *ep* collisions at HERA

ZEUS Collaboration

Abstract

A search has been made for lepton-flavor-violating interactions of the type $ep \to \mu X$, with the ZEUS detector at HERA using an integrated luminosity of 130 pb^{-1}. The data were taken at a center-of-mass energies, $\sqrt{s}$, of 300 and 318 GeV. No evidence was found for lepton-flavor violation and constraints were derived on leptoquarks (LQs) that could mediate such interactions. For LQ masses below $\sqrt{s}$, limits are set on $\lambda_{eq_1}\sqrt{\beta_{\mu q}}$, where λ_{eq_1} is the coupling of the LQ to an electron and a first-generation quark q_1, and $\beta_{\mu q}$ is the branching ratio of the LQ to μ and a quark. For LQ masses exceeding $\sqrt{s}$, limits are set on the four-fermion contact-interaction term $\lambda_{eq_\alpha}\lambda_{\mu q_\beta}/M_{\rm LQ}^2$ for leptoquarks that couple to an electron and a quark q_α and also to μ and a quark q_β. Some of the limits are also applicable to lepton-flavor-violating processes mediated by squarks in R-parity-violating supersymmetric models. In some cases involving heavy quarks, the ZEUS limits are the most stringent published to date.

1 Introduction

In the Standard Model (SM), lepton flavor is conserved. While the reported observation of neutrino oscillations [1,2] implies that lepton-flavor violation (LFV) does occur, minimal extensions to the SM [3] that allow for finite neutrino masses and thereby account for neutrino oscillations do not predict detectable rates of LFV at current collider experiments. However, many extensions of the SM, such as grand unified theories [4], models based on supersymmetry [5], compositeness [6] or technicolor [7] involve LFV interactions at fundamental levels.

In high-energy ep collisions at HERA, reactions of the type $eq_i \to \mu q_f$, where q_i and q_f denote initial- and final-state quarks and the final state μ has large transverse momentum, can be detected with high efficiency and small background. Such reactions, shown in Fig. 1 in case of a positron beam, can be induced by leptoquarks (LQs), bosons that carry both lepton (L) and baryon (B) numbers and have lepton-quark Yukawa couplings. Such bosons arise naturally in unified theories that arrange quarks and leptons in common multiplets. A LQ that couples to leptons of two different generations would induce LFV. The Buchmüller-Rückl-Wyler (BRW) model [8] was used in order to classify LQ species and to evaluate cross sections of the LQ–induced processes. These processes can also be mediated by squarks in R–parity–violating SUSY models. Further details on these models and on the cross–section approximation used are reported elsewhere [9].

Indirect searches for the above reactions have yielded very strong constraints [10] for cases where q_i and q_f are light quarks. However, in some cases involving heavy quarks, the sensitivity of HERA extends beyond existing low-energy limits.

This paper reports on a search for LFV processes in e^+p collisions using data collected by the ZEUS experiment from 1999 to 2000 at a center–of–mass energy, $\sqrt{s}$, of 318 GeV with an integrated luminosity, $\mathcal{L}$, of 65.5 pb^{-1}. Final results for limit settings have been obtained by combining the constraints from this analysis with the ZEUS limits [9,11] from the previous running periods. Limits for low–mass LQs ($M_{LQ} < \sqrt{s}$) have been obtained using the whole e^+p data sample for an integrated luminosity of 113.2 pb^{-1}. For high–mass LQs ($M_{LQ} \gg \sqrt{s}$) the whole $e^{\pm}p$ data sample collected in the HERA I phase, a total integrated luminosity of 129.9 pb^{-1}, was used. Previous searches for LFV at HERA have been reported by ZEUS [9,11,12] and H1 [13].

2 Event selection

Events from the reaction $ep \to \mu X$, mediated by a heavy LQ, would be characterized by a high-transverse-momentum (P_t) muon balanced by a jet. Since only a small fraction of the muon energy is deposited in the calorimeter, the event selection is mainly based on the requirement of a large missing transverse momentum ($\not{P}_t$) as measured by the calorimeter.

A detailed description of the ZEUS detector can be found elsewhere [14]. The main component used for this analysis are the central tracking detector (CTD) [15], the uranium calorimeter (CAL) [16], the forward muon detector (FMUON) [14] and the luminosity monitor [17,18]. Global calorimeter sums, used in the event selection, were calculated as follows: to each calorimeter cell i with an energy deposit E_i above a threshold was assigned a four-momentum P^μ, defined as $P^\mu = (E_i, E_i \cos\phi_i \sin\theta_i, E_i \sin\phi_i \sin\theta_i, E_i \cos\theta_i)$, where ϕ_i and θ_i are the azimuthal and polar angles of the cell center relative to the event vertex[1]. The total four-momentum seen by the calorimeter (E, P_X, P_Y, P_Z) is given by the sum of the four-momenta for all cells. The transverse energy, E_t, is given by $\sum_i E_i \sin\theta_i$. The missing transverse momentum, $\not{P}_t$, is given by $\sqrt{P_X^2 + P_Y^2}$. The azimuthal angle assigned to $\not{P}_t$, ϕ_{miss}, was defined by $\cos\phi_{\text{miss}} = -P_X/\not{P}_t$ and $\sin\phi_{\text{miss}} = -P_Y/\not{P}_t$.

The $E - P_Z$ of the initial state is twice the positron beam energy, $2E_e = 55\,\text{GeV}$. For events that are fully contained in the calorimeter (ignoring particles escaping through the forward beam hole, which carry negligible $E - P_Z$), the measured $E - P_Z$ should be near $2E_e$. In photoproduction processes, where the final-state positron escapes through the rear beam hole, the $E - P_Z$ spectrum falls steeply, so that a cut on $E - P_Z$ is useful in reducing such backgrounds. Events with high-energy muons, which deposit only a small fraction of their energy in the calorimeter, will also have $E - P_Z$ substantially below $2E_e$. In the search for the $e \to \mu$ transition, a cut was made on the quantity $E - P_Z + \Delta_\mu$, where $\Delta_\mu = \not{P}_t(1 - \cos\theta_\mu)/\sin\theta_\mu$ is an estimate of the $E - P_Z$ carried by the muon, assuming that the transverse momentum of the muon is equal to $\not{P}_t$; θ_μ is the polar angle of the muon track.

2.1 Trigger and preselection

The trigger, which is identical to that used in the CC DIS measurement described elsewhere [19], was based on a cut on $\not{P}_t$ with a considerably lower threshold than the selection cuts described below. After applying cuts to reject non-ep backgrounds (mainly cosmic rays and beam-gas interactions), the following pre-selection requirements were imposed:

- a reconstructed vertex with Z coordinate $|Z_{\text{VTX}}| < 50\,\text{cm}$;
- $\not{P}_t > 15\,\text{GeV}$;

[1] The ZEUS coordinate system is a right-handed Cartesian system, with the Z axis pointing in the proton beam direction, referred to as the "forward direction", and the X axis pointing left towards the center of HERA. The coordinate origin is at the nominal interaction point.

- no electron with energy larger than 10 GeV;
- $\not{P}_t/\sqrt{E_t} > 3\sqrt{\mathrm{GeV}}$;
- an isolated μ candidate in the $\not{P}_t$ direction (described below).

The third cut, where the electron finder [20] is based on a neural–network algorithm, reject NC DIS. The muon identification was performed using two methods. The first, for very forward muons ($8^\circ < \theta_\mu < 20^\circ$), required a reconstructed track in the FMUON detector with azimuth within 20° of ϕ_{miss}. In the second selection, for central muons ($15^\circ < \theta_\mu < 164^\circ$), the following CAL- and CTD-based requirements were imposed:

- a track that pointed to the vertex with transverse momentum (P_t^{trk}) above 5 GeV and an azimuth that differed from ϕ_{miss} by less than 20°;
- the calorimeter energy deposits, associated with the track, were consistent with those expected from a minimum ionizing particle;
- $D_{trk} > 0.5$ and $D_{jet} > 1$, where D_{trk} and D_{jet} are the distances in the η-ϕ plane of the closest track and jet, respectively.

The SM expectations have been evaluated using Monte Carlo (MC) generators which simulate the main sources of background for a LFV signal. Neutral and charged current deep inelastic scattering, W production, QED di–muon and di–tau production, direct and resolved photoproduction processes have been considered. Figure 2 shows the data-MC comparison after the pre–selection. Eighteen events were left in the data, while the SM expectation is 14.8 ± 0.9, mainly from the QED di–muon process ($ep \to e\mu^+\mu^- X$). This process has been generated using GRAPE [21].

2.2 Final selection

The final selection was designed to reduce the SM background to a very low level. The following further cuts were applied:

- $\not{P}_t > 20\,\mathrm{GeV}$;
- $E - P_Z + \Delta_\mu > 45\,\mathrm{GeV}$.

No event survived these cuts, while 0.35 ± 0.10 are predicted by SM processes, mostly from $ep \to e\mu^+\mu^- X$.

3 Results

The selection efficiencies were evaluated using signal MC events generated by LQGENEP 1.0 [22]. For resonant production of lepton-flavor-violating scalar LQs, the selection efficiency falls from 55% to 40% as $M_{\rm LQ}$ increases from 140 GeV to 300 GeV, while the efficiency for vector LQs drops from 63% to 50%.

For LQs with $M_{\rm LQ} \gg \sqrt{s}$, the efficiencies are almost independent of $M_{\rm LQ}$, but depend strongly on the generation of the initial-state quark. The selection efficiency ranges from 48% to 28% for $F = 0$ ($F = 3B + L$ is the LQ fermionic number) LQs and from 45% to 29% for $|F| = 2$ LQs. When the initial-state quark is a sea quark and especially for s, c, or b quarks, the efficiency is considerably lower than for valence quarks, due to the softer x spectrum, which results in a lower transverse momentum for the final-state muon.

Since no candidate was found, limits at 95% C.L. were set on the LFV process $e^+p \to \mu X$. LQs with mass less than $\sqrt{s}$ are predominantly produced as narrow resonances in the s-channel. The branching ratio of the LQ to μq, β, was regarded as a free parameter and limits were set on $\sigma\beta_{\mu q}$. Figure 3 shows upper limits on $\sigma\beta_{\mu q}$; the search is sensitive to processes with cross sections as low as 0.08 pb.

These limits were then converted into limits on $\lambda_{eq_1}\sqrt{\beta_{\mu q}}$ using the narrow–width approximation for the cross section corrected for QED initial-state radiation (ISR) and next-to-leading-order QCD effects [23, 24] (only for scalar LQs). For leptoquarks with mass greater than $\sqrt{s}$, the cross-section limit was converted to a limit on $\lambda_{eq_\alpha}\lambda_{\mu q_\beta}/M^2_{\rm LQ}$ ($M_{\rm LQ}$ is the LQ mass, α and β denote the quark generations) using the contact–interaction approximation with QED-ISR corrections. The CTEQ5 [25] parameterizations of parton densities were used to evaluate cross sections.

3.1 Low-mass LQ and squark limits

The limits presented in this section have been obtained by combining the results of this analysis with the 94-97 e^+p ZEUS limits [9], thereby corresponding to a total integrated luminosity of 113.2 pb^{-1}.

Upper limits on $\lambda_{eq_1}\sqrt{\beta_{\mu q}}$ have been derived for F=0 LQs by assuming resonant production of LQs described by the BRW model. These limits can be applied to processes involving any quark generations in the final state (excluding the $t-$quark). Figures 4(a-b) show the upper limits on $\lambda_{eq_1}\sqrt{\beta_{\mu q}}$ for scalar and vector LQs, respectively. Under the assumption that $\lambda_{eq_1} = \lambda_{\mu q_\beta}$, limits on λ_{eq_1} can be derived. These are compared to limits from low-energy experiments in Figs. 4(c-d) for $\tilde{S}^L_{1/2}$ and V^R_0 LQs. These states do not couple to neutrinos and therefore $\beta_{\mu q} = 0.5$. For $M_{\rm LQ} < 250$ GeV, the ZEUS limits are stronger than the low-energy limits for LQs that couple to μ and b. The limits on $\lambda_{eq_1}\sqrt{\beta_{\mu q}}$ for $\tilde{S}^L_{1/2}$ can be interpreted as limits on $\lambda'_{1j1}\sqrt{\beta_{\tilde{u}^j\to\mu q}}$ for $\tilde{u}^j$ squarks.

Another way to illustrate the sensitivity is to assume that the couplings have electromagnetic strength ($\lambda_{eq_1} = \lambda_{\mu q_\beta} = 0.3 \approx \sqrt{4\pi\alpha}$). In this case, LQs with masses up to 301 GeV are excluded, as shown in Table 1. Alternatively, as shown in Table 2, for a fixed M_{LQ} of 250 GeV, values of $\lambda_{eq_1}\sqrt{\beta_{\mu q}}$ down to 0.0094 are excluded.

The CDF [26] and DØ [27] collaborations exclude scalar LQs with $M_{\mathrm{LQ}} < 202\,\mathrm{GeV}$ and $M_{\mathrm{LQ}} < 200\,\mathrm{GeV}$, respectively, at 95% C.L. with $\beta_{\mu q} = 100\%$. CDF [28] excludes $M_{\mathrm{LQ}} < 99\,\mathrm{GeV}$ with $\beta_{\tau b} = 100\%$. The ZEUS limits are complementary to those of the Tevatron in the sense that the latter are independent of the Yukawa couplings but assume that LQs couple to a single lepton generation.

3.2 High-mass LQ and squark limits

The limits presented in this section have been obtained combining the results of this analysis with the 94-97 e^+p [9] and 98-99 e^-p ZEUS limits [11], thereby corresponding to a total integrated luminosity of $129.9\,\mathrm{pb}^{-1}$. For $M_{\mathrm{LQ}} \gg \sqrt{s}$, limits on $\lambda_{eq_\alpha}\lambda_{\mu q_\beta}/M_{\mathrm{LQ}}^2$ were evaluated for all combinations of quark generations (α, β). Tables 3 and 4 show these limits for $F = 0$ and $|F| = 2$ LQs, respectively. In some cases involving c and b quarks, the ZEUS limits improve on the low-energy limits [10, 29, 30]. Limits obtained by H1 [13] are comparable to the ZEUS limits.

The limits on $\lambda_{eq_\alpha}\lambda_{\mu q_\beta}/M_{\mathrm{LQ}}^2$ for $\tilde{S}^L_{1/2}$ can be interpreted as limits on $\lambda'_{1j\alpha}\lambda'_{2j\beta}/M^2_{\tilde{u}}$ for a u-type squark of generation j. Similarly, the limits on S^L_0 LQs can be interpreted as limits on $\lambda'_{1\alpha k}\lambda'_{2\beta k}/M^2_{\tilde{d}}$ for a d-type squark of generation k.

4 Conclusions

A search for lepton-flavor violation has been performed with $130\,\mathrm{pb}^{-1}$ of ep data at $\sqrt{s} = 300\,\mathrm{GeV}$ and $318\,\mathrm{GeV}$ collected with the ZEUS detector at HERA in 1994–2000. No evidence for LFV processes has been found.

Limits at 95% C.L. on cross sections, couplings and masses for F=0 leptoquarks that mediate LFV processes have been set. Assuming the couplings $\lambda_{eq_1} = \lambda_{\ell q_\beta} = 0.3$, lower mass limits between 280 and 301 GeV have been derived for various LQs decaying to μq. For $M_{\mathrm{LQ}} = 250\,\mathrm{GeV}$, upper limits for $\lambda_{eq_1}\sqrt{\beta_{\mu q}}$ in the range $(0.94-4.5)\cdot 10^{-2}$ were obtained. Limits on $\tilde{S}^L_{1/2}$ also apply to up-type squarks that have R-parity-violating couplings to a positron and a μ.

For LQs with $M_{\mathrm{LQ}} \gg \sqrt{s}$, upper limits on $\lambda_{eq_\alpha}\lambda_{\mu q_\beta}/M_{\mathrm{LQ}}^2$ have been obtained and compared with bounds from low-energy experiments. Some of these limits also apply to high-mass R_p-violating squarks. Some of the ZEUS limits, when higher–generation quarks are involved, are the most stringent published to date.

References

[1] Super-Kamiokande Coll., Y. Fukuda et al., Phys. Rev. Lett. **81**, 1562 (1998).

[2] SNO Coll., Q.R. Ahmad et al., Phys. Rev. Lett. **87**, 071301 (2001).

[3] Z. Maki, M. Nakagawa and S. Sakata, Prog. Theor. Phys. **28**, 870 (1962); P. Fisher, B. Kayser and K.S. McFarland, Ann. Rev. Nucl. Part. Sci. **49**, 481 (1999).

[4] J.C. Pati and A. Salam, Phys. Rev. **D 10**, 275 (1974); H. Georgi and S.L. Glashow, Phys. Rev. Lett. **32**, 438 (1974); P. Langacker, Phys. Rep. **72**, 185 (1981).

[5] H.P. Nilles, Phys. Rep. **110**, 1 (1984); H.E. Haber and G.L. Kane, Phys. Rep. **117**, 75 (1985).

[6] B. Schrempp and F. Schrempp, Phys. Lett. **B 153**, 101 (1985); J. Wudka, Phys. Lett. **B 167**, 337 (1986).

[7] S. Dimopoulos and L. Susskind, Nucl. Phys. **B 155**, 237 (1979); S. Dimopoulos, Nucl. Phys. **B 168**, 69 (1980); E. Farhi and L. Susskind, Phys. Rev. **D 20**, 3404 (1979); E. Farhi and L. Susskind, Phys. Rep. **74**, 277 (1981).

[8] W. Buchmüller, R. Rückl and D. Wyler, Phys. Lett. **B 191**, 442 (1987). Erratum in Phys. Lett. **B 448**, 320 (1999).

[9] ZEUS Coll., S. Chekanov et al., Phys. Rev. **D 65**, 92004 (2002).

[10] S. Davidson, D. Bailey and B.A. Campbell, Z. Phys. **C 61**, 613 (1994).

[11] ZEUS Coll., *Search for lepton-flavor violation in ep collisions at HERA*. Paper 605 submitted to the International Europhysics Conference on High Energy Physics 01, Budapest, Hungary, July 12-18, 2001.

[12] ZEUS Coll., M. Derrick et al., Z. Phys. **C 73**, 613 (1997).

[13] H1 Coll., C. Adloff et al., Eur. Phys. J. **C 11**, 447 (1999). Erratum in Eur. Phys. J. C14, 553 (2000).

[14] ZEUS Coll., U. Holm (ed.), *The ZEUS Detector*. Status Report (unpublished), DESY (1993), available on `http://www-zeus.desy.de/bluebook/bluebook.html`.

[15] N. Harnew et al., Nucl. Inst. Meth. **A 279**, 290 (1989); B. Foster et al., Nucl. Phys. Proc. Suppl. **B 32**, 181 (1993); B. Foster et al., Nucl. Inst. Meth. **A 338**, 254 (1994).

[16] M. Derrick et al., Nucl. Inst. Meth. **A 309**, 77 (1991);
A. Andresen et al., Nucl. Inst. Meth. **A 309**, 101 (1991);
A. Caldwell et al., Nucl. Inst. Meth. **A 321**, 356 (1992);
A. Bernstein et al., Nucl. Inst. Meth. **A 336**, 23 (1993).

[17] J. Andruszków et al., Preprint DESY-92-066, DESY, 1992;
ZEUS Coll., M. Derrick et al., Z. Phys. **C 63**, 391 (1994).

[18] J. Andruszków et al., Acta Phys. Pol. **B 32**, 2025 (2001).

[19] ZEUS Coll., J. Breitweg et al., Eur. Phys. J. **C 12**, 411 (2000).

[20] H. Abramowicz, A. Caldwell and R. Sinkus, Nucl. Inst. Meth. **A 365**, 508 (1995).

[21] T. Abe, Comp. Phys. Comm. **136**, 126 (2001).

[22] L. Bellagamba, Comp. Phys. Comm. **141**, 83 (2001).

[23] T. Plehn et al., Z. Phys. **C 74**, 611 (1997).

[24] Z. Kunszt and W.J. Stirling, Z. Phys. **C 75**, 453 (1997).

[25] CTEQ Coll., H.L. Lai et al., Eur. Phys. J. **C 12**, 375 (2000).

[26] CDF Coll., F. Abe et al., Phys. Rev. Lett. **81**, 4806 (1998).

[27] DØ Coll., B. Abbott et al., Phys. Rev. Lett. **84**, 2088 (2000).

[28] CDF Coll., F. Abe et al., Phys. Rev. Lett. **78**, 2906 (1997).

[29] E. Gabrielli, Phys. Rev. **D 62**, 055009 (2000).

[30] Particle Data Group, D.E. Groom et al., Eur. Phys. J. **C 15**, 1 (2000).

LQ type	$\tilde{S}^L_{1/2}$	$S^L_{1/2}$	$S^R_{1/2}$	V^L_0	V^R_0	$\tilde{V}^R_0$	V^L_1
μ-channel limit on $M_{\rm LQ}$[GeV]	280	296	296	279	284	298	301

Table 1: *The 95% C.L. lower limits on $M_{\rm LQ}$ assuming $\lambda_{eq_1} = \lambda_{\ell q} = 0.3$.*

LQ type	$\tilde{S}^L_{1/2}$	$S^L_{1/2}$	$S^R_{1/2}$	V^L_0/V^R_0	$\tilde{V}^R_0$	V^L_1
μ-channel limit on $\lambda_{eq_1}\sqrt{\beta_{\mu q}}$	0.045	0.019	0.017	0.033	0.014	0.0094

Table 2: *The 95% C.L. upper limits on $\lambda_{eq_1}\sqrt{\beta_{\mu q}}$ for a leptoquark with mass $M_{\rm LQ} = 250\,GeV$.*

$e \to \mu$ ZEUS (prel.) ep 94-00 $F=0$							
$\alpha\beta$	$S^L_{1/2}$ e^+u_α	$S^R_{1/2}$ $e^+(u+d)_\alpha$	$\tilde{S}^L_{1/2}$ e^+d_α	V^L_0 e^+d_α	V^R_0 e^+d_α	$\tilde{V}^R_0$ e^+u_α	V^L_1 $e^+(\sqrt{2}u+d)_\alpha$
1 1	$\mu N \to eN$ 7.6×10^{-5} **1.1**	$\mu N \to eN$ 2.6×10^{-5} **0.9**	$\mu N \to eN$ 7.6×10^{-5} **1.6**	$\mu N \to eN$ 2.6×10^{-5} **1.0**	$\mu N \to eN$ 2.6×10^{-5} **1.0**	$\mu N \to eN$ 2.6×10^{-5} **0.8**	$\mu N \to eN$ 1.1×10^{-5} **0.4**
1 2	$D \to \mu\bar{e}$ 4 $\boxed{\mathbf{1.2}}$	$K \to \mu\bar{e}$ 2.7×10^{-5} **1.0**	$K \to \mu\bar{e}$ 2.7×10^{-5} **1.7**	$K \to \mu\bar{e}$ 1.3×10^{-5} **1.2**	$K \to \mu\bar{e}$ 1.3×10^{-5} **1.2**	$D \to \mu\bar{e}$ 2 $\boxed{\mathbf{1.0}}$	$K \to \mu\bar{e}$ 1.3×10^{-5} **0.5**
1 3	*	$B \to \mu\bar{e}$ 0.8 **1.8**	$B \to \mu\bar{e}$ 0.8 **1.8**	V_{ub} 0.2 **1.5**	$B \to \mu\bar{e}$ 0.4 **1.5**	*	V_{ub} 0.2 **1.5**
2 1	$D \to \mu\bar{e}$ 4 $\boxed{\mathbf{3.6}}$	$K \to \mu\bar{e}$ 2.7×10^{-5} **2.4**	$K \to \mu\bar{e}$ 2.7×10^{-5} **3.2**	$K \to \mu\bar{e}$ 1.3×10^{-5} **1.3**	$K \to \mu\bar{e}$ 1.3×10^{-5} **1.3**	$D \to \mu\bar{e}$ 2 $\boxed{\mathbf{1.3}}$	$K \to \mu\bar{e}$ 1.3×10^{-5} **0.6**
2 2	$\mu \to ee\bar{e}$ 5×10^{-3} **5.8**	$\mu \to ee\bar{e}$ 7.3×10^{-3} **3.1**	$\mu \to ee\bar{e}$ 1.6×10^{-2} **3.8**	$\mu \to ee\bar{e}$ 8×10^{-3} **1.9**	$\mu \to ee\bar{e}$ 8×10^{-3} **1.9**	$\mu \to ee\bar{e}$ 2.5×10^{-3} **2.9**	$\mu \to ee\bar{e}$ 1.5×10^{-3} **1.2**
2 3	*	$B \to \bar{\mu}eK$ 0.6 **4.3**	$B \to \bar{\mu}eK$ 0.6 **4.3**	$B \to \bar{\mu}eK$ 0.3 **2.9**	$B \to \bar{\mu}eK$ 0.3 **2.9**	*	$B \to \bar{\mu}eK$ 0.3 **2.9**
3 1	*	$B \to \mu\bar{e}$ 0.8 **4.4**	$B \to \mu\bar{e}$ 0.8 **4.4**	V_{ub} 0.2 **1.5**	$B \to \mu\bar{e}$ 0.4 **1.5**	*	V_{ub} 0.2 **1.5**
3 2	*	$B \to \bar{\mu}eK$ 0.6 **5.8**	$B \to \bar{\mu}eK$ 0.6 **5.8**	$B \to \bar{\mu}eK$ 0.3 **2.2**	$B \to \bar{\mu}eK$ 0.3 **2.2**	*	$B \to \bar{\mu}eK$ 0.3 **2.2**
3 3	*	$\mu \to ee\bar{e}$ 7.3×10^{-3} **7.7**	$\mu \to ee\bar{e}$ 1.6×10^{-2} **7.7**	$\mu \to ee\bar{e}$ 8×10^{-3} **3.9**	$\mu \to ee\bar{e}$ 8×10^{-3} **3.9**	*	$\mu \to ee\bar{e}$ 1.5×10^{-3} **3.9**

Table 3: *Upper limits at 95% C.L. on* $\lambda_{eq_\alpha}\lambda_{\mu q_\beta}/M^2_{LQ}$ *in units of* TeV^{-2}, *for* $F=0$ *LQs that couple to* eq_α *and to* μq_β. *The columns correspond to the* $F=0$ *LQ species. The* eq_α *combination for* e^+p *collisions and s-channel case is reported under the LQ type (the combination for* e^-p *collisions can be obtained by applying charge conjugation). Each row corresponds to a different combination of quark generations* (α,β) *that couple to the* e *and the* μ, *respectively. Within each cell, the measurement that provides the most stringent low–energy constraint is shown on the first line and the corresponding limit [10, 29, 30] is given on the second line. The ZEUS limits are shown on the third line of each cell (enclosed in a box when stronger than the low–energy constraint). The * indicates cases where a top quark must be involved.*

$e \to \mu$	ZEUS (prel.) ep 94-00			$\lvert F\rvert = 2$			
$\boldsymbol{\alpha\beta}$	$\boldsymbol{S_0^L}$ $e^+\bar{u}_\alpha$	$\boldsymbol{S_0^R}$ $e^+\bar{u}_\alpha$	$\boldsymbol{\tilde{S}_0^R}$ $e^+\bar{d}_\alpha$	$\boldsymbol{S_1^L}$ $e^+(\bar{u}+\sqrt{2}\bar{d})_\alpha$	$\boldsymbol{V_{1/2}^L}$ $e^+\bar{d}_\alpha$	$\boldsymbol{V_{1/2}^R}$ $e^+(\bar{u}+\bar{d})_\alpha$	$\boldsymbol{\tilde{V}_{1/2}^L}$ $e^+\bar{u}_\alpha$
1 1	$\boldsymbol{\mu N \to eN}$ 7.6×10^{-5} **1.6**	$\boldsymbol{\mu N \to eN}$ 7.6×10^{-5} **1.6**	$\boldsymbol{\mu N \to eN}$ 7.6×10^{-5} **2.1**	$\boldsymbol{\mu N \to eN}$ 2.3×10^{-5} **0.9**	$\boldsymbol{\mu N \to eN}$ 2.6×10^{-5} **0.9**	$\boldsymbol{\mu N \to eN}$ 1.3×10^{-5} **0.5**	$\boldsymbol{\mu N \to eN}$ 2.6×10^{-5} **0.6**
1 2	$\boldsymbol{K \to \pi\nu\bar{\nu}}$ 10^{-3} **2.4**	$\boldsymbol{D \to \mu\bar{e}}$ 4 $\boxed{\mathbf{2.4}}$	$\boldsymbol{K \to \mu\bar{e}}$ 2.7×10^{-5} **2.6**	$\boldsymbol{K \to \mu\bar{e}}$ 1.3×10^{-5} **1.1**	$\boldsymbol{K \to \mu\bar{e}}$ 1.3×10^{-5} **1.6**	$\boldsymbol{K \to \mu\bar{e}}$ 1.3×10^{-5} **1.2**	$\boldsymbol{D \to \mu\bar{e}}$ 2 $\boxed{\mathbf{1.7}}$
1 3	$\boldsymbol{V_{ub}}$ 0.4 *	*	$\boldsymbol{B \to \mu\bar{e}}$ 0.8 **2.8**	$\boldsymbol{V_{ub}}$ 0.4 **1.4**	$\boldsymbol{B \to \mu\bar{e}}$ 0.4 **2.1**	$\boldsymbol{B \to \mu\bar{e}}$ 0.4 **2.1**	*
2 1	$\boldsymbol{K \to \pi\nu\bar{\nu}}$ 10^{-3} **2.1**	$\boldsymbol{D \to \mu\bar{e}}$ 4 $\boxed{\mathbf{2.1}}$	$\boldsymbol{K \to \mu\bar{e}}$ 2.7×10^{-5} **2.6**	$\boldsymbol{K \to \mu\bar{e}}$ 1.3×10^{-5} **1.1**	$\boldsymbol{K \to \mu\bar{e}}$ 1.3×10^{-5} **0.9**	$\boldsymbol{K \to \mu\bar{e}}$ 1.3×10^{-5} **0.5**	$\boldsymbol{D \to \mu\bar{e}}$ 2 $\boxed{\mathbf{0.6}}$
2 2	$\boldsymbol{\mu \to ee\bar{e}}$ 5×10^{-3} **5.7**	$\boldsymbol{\mu \to ee\bar{e}}$ 5×10^{-3} **5.7**	$\boldsymbol{\mu \to ee\bar{e}}$ 1.6×10^{-2} **3.8**	$\boldsymbol{\mu \to ee\bar{e}}$ 1.3×10^{-2} **1.8**	$\boldsymbol{\mu \to ee\bar{e}}$ 8×10^{-3} **1.9**	$\boldsymbol{\mu \to ee\bar{e}}$ 3.7×10^{-3} **1.6**	$\boldsymbol{\mu \to ee\bar{e}}$ 2.5×10^{-3} **2.9**
2 3	$\boldsymbol{B \to l\nu X}$ 4 *	*	$\boldsymbol{B \to \bar{\mu}eK}$ 0.6 **4.3**	$\boldsymbol{B \to \bar{\mu}eK}$ 0.3 **2.1**	$\boldsymbol{B \to \bar{\mu}eK}$ 0.3 **2.9**	$\boldsymbol{B \to \bar{\mu}eK}$ 0.3 **2.9**	*
3 1	$\boldsymbol{V_{ub}}$ 0.4 *	*	$\boldsymbol{B \to \mu\bar{e}}$ 0.8 **3.1**	$\boldsymbol{V_{ub}}$ 0.4 **1.5**	$\boldsymbol{B \to \mu\bar{e}}$ 0.4 **1.0**	$\boldsymbol{B \to \mu\bar{e}}$ 0.4 **1.0**	*
3 2	$\boldsymbol{B \to l\nu X}$ 4 *	*	$\boldsymbol{B \to \bar{\mu}eK}$ 0.6 **5.8**	$\boldsymbol{B \to \bar{\mu}eK}$ 0.3 **2.9**	$\boldsymbol{B \to \bar{\mu}eK}$ 0.3 **2.2**	$\boldsymbol{B \to \bar{\mu}eK}$ 0.3 **2.2**	*
3 3	*	*	$\boldsymbol{\mu \to ee\bar{e}}$ 1.6×10^{-2} **7.6**	$\boldsymbol{\mu \to ee\bar{e}}$ 1.3×10^{-2} **3.8**	$\boldsymbol{\mu \to ee\bar{e}}$ 8×10^{-3} **4.0**	$\boldsymbol{\mu \to ee\bar{e}}$ 3.7×10^{-3} **4.0**	*

Table 4: *Upper limits at 95% C.L. on $\lambda_{eq_\alpha}\lambda_{\mu q_\beta}/M_{LQ}^2$ in units of* TeV^{-2}*, for $|F| = 2$ LQs that couple to eq_α and to μq_β. The columns correspond to the $|F| = 2$ LQ species. The format of the table is described in the caption of Table 3.*

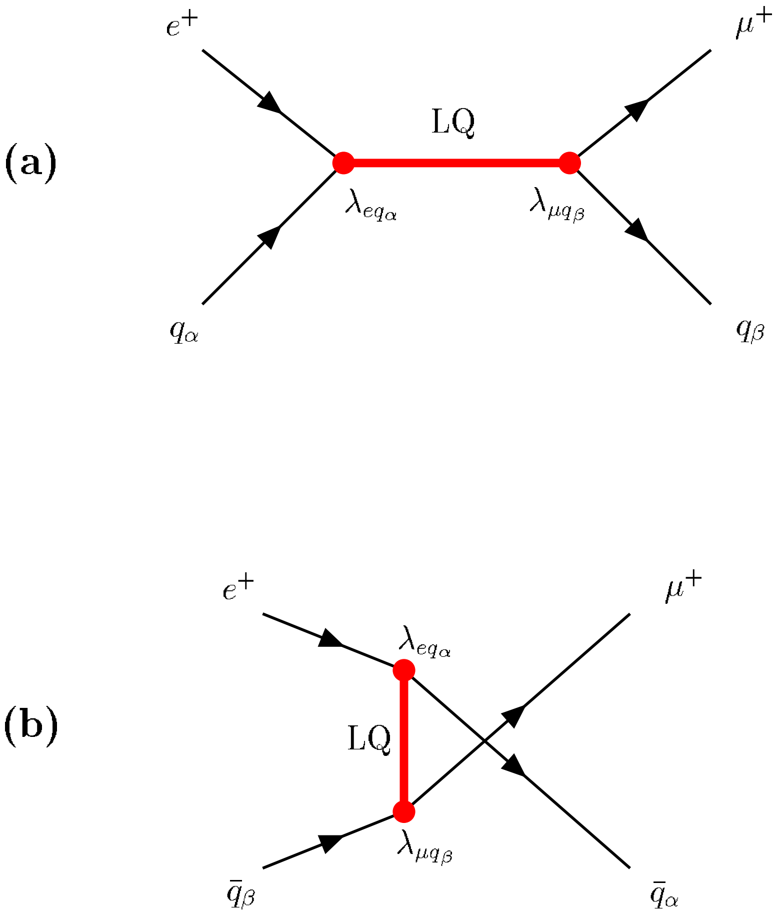

Figure 1: *(a) s-channel and (b) u-channel diagrams contributing to LFV processes induced by $F = 0$ LQs, where $F = 3B + L$ is the LQ fermionic number, B and L being baryon and lepton numbers, respectively. The subscripts α and β denote the quark generations. In e^+p scattering, $|F| = 2$ LQs couple to antiquarks in the s-channel and to quarks in the u-channel.*

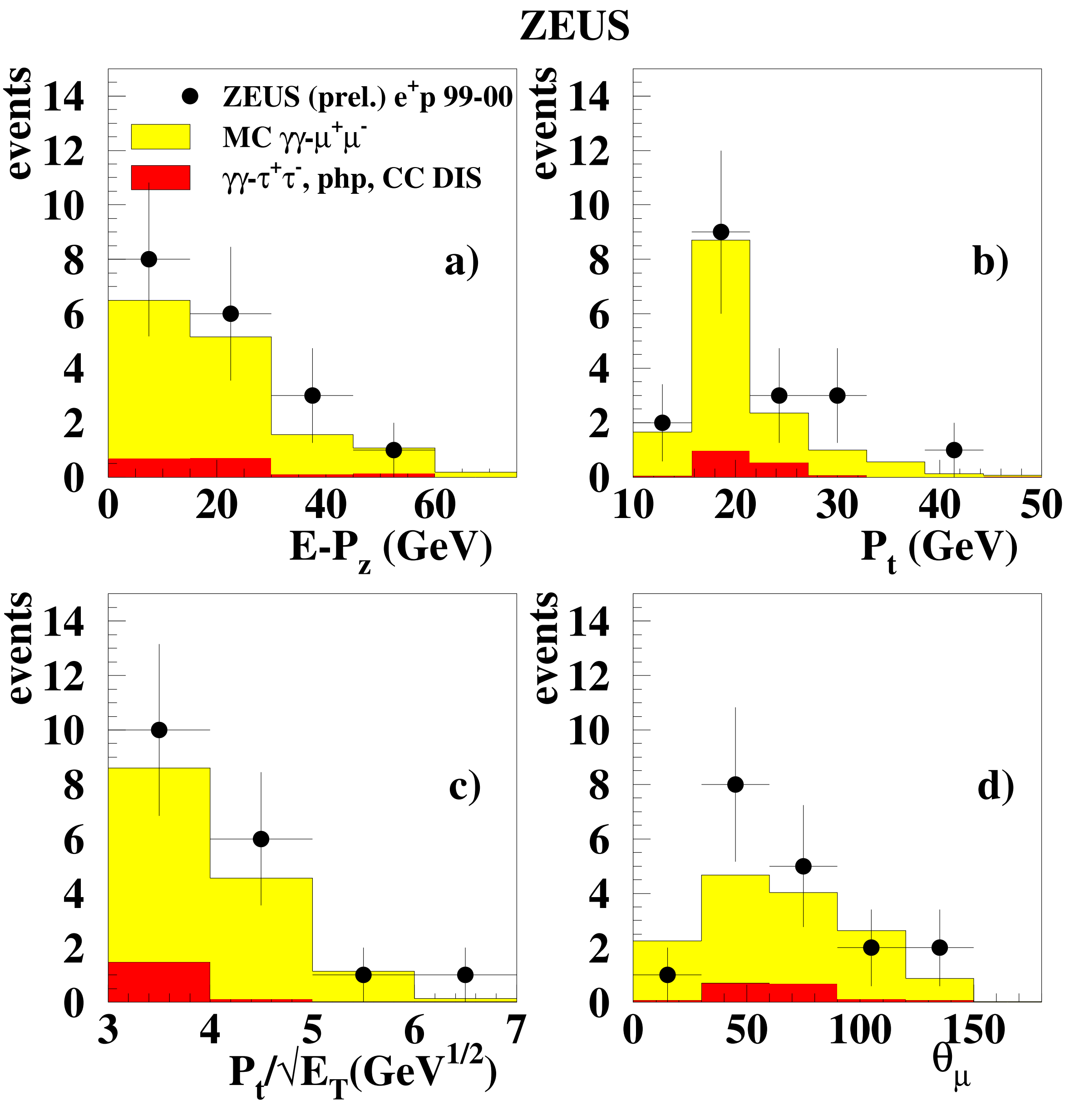

Figure 2: *Distributions of event variables after muon identification for data (solid points) and SM simulation (histograms) for a)* $E - P_Z + \Delta_\mu$*, b)* $\not{P}_t$*, c)* $\not{P}_t/\sqrt{E_t}$ *and d)* θ_μ*.*

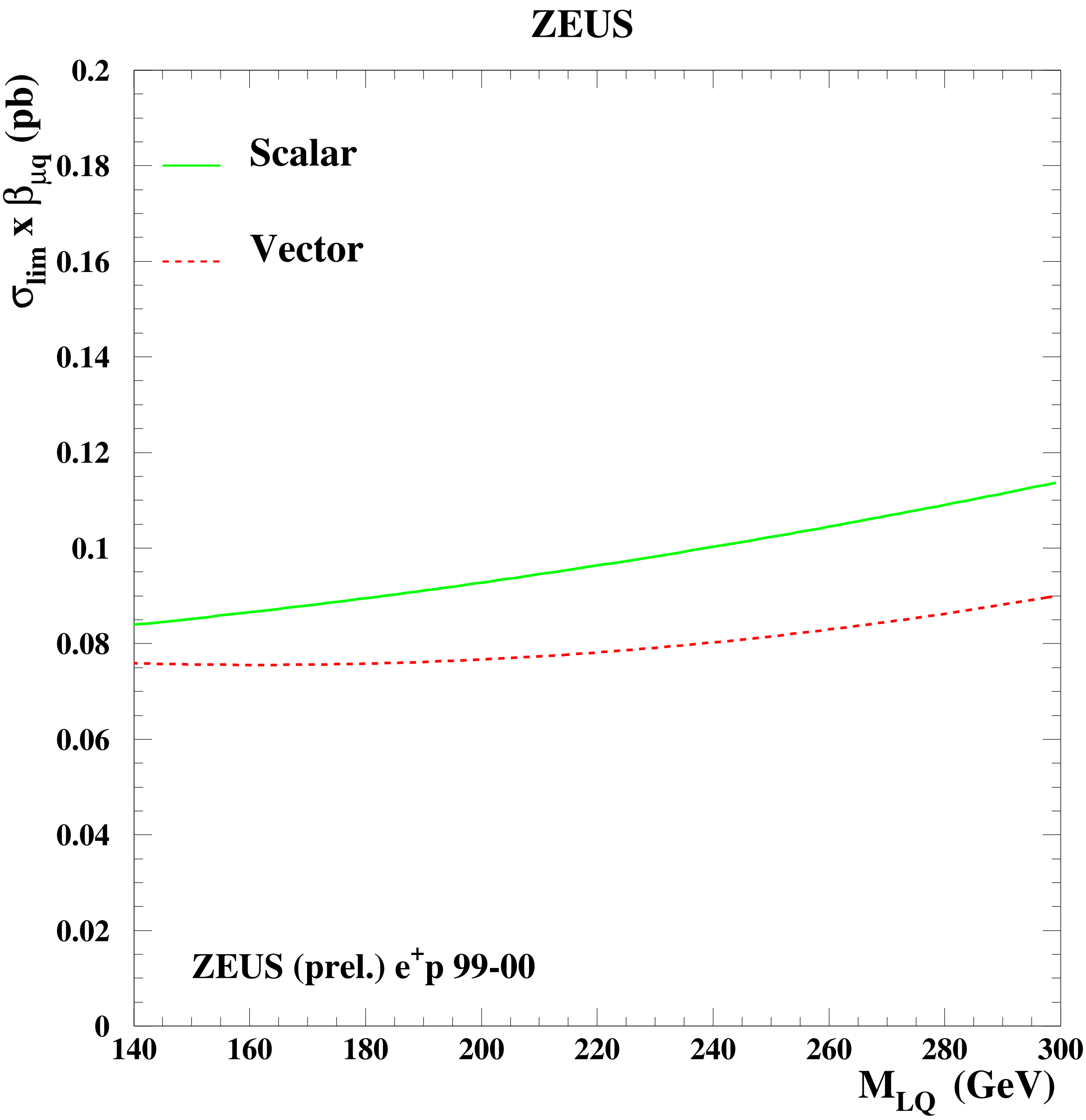

Figure 3: *The 95% C.L. upper limits on $\sigma\beta_{\mu q}$ as a function of $M_{\rm LQ}$ for scalar and vector LQ.*

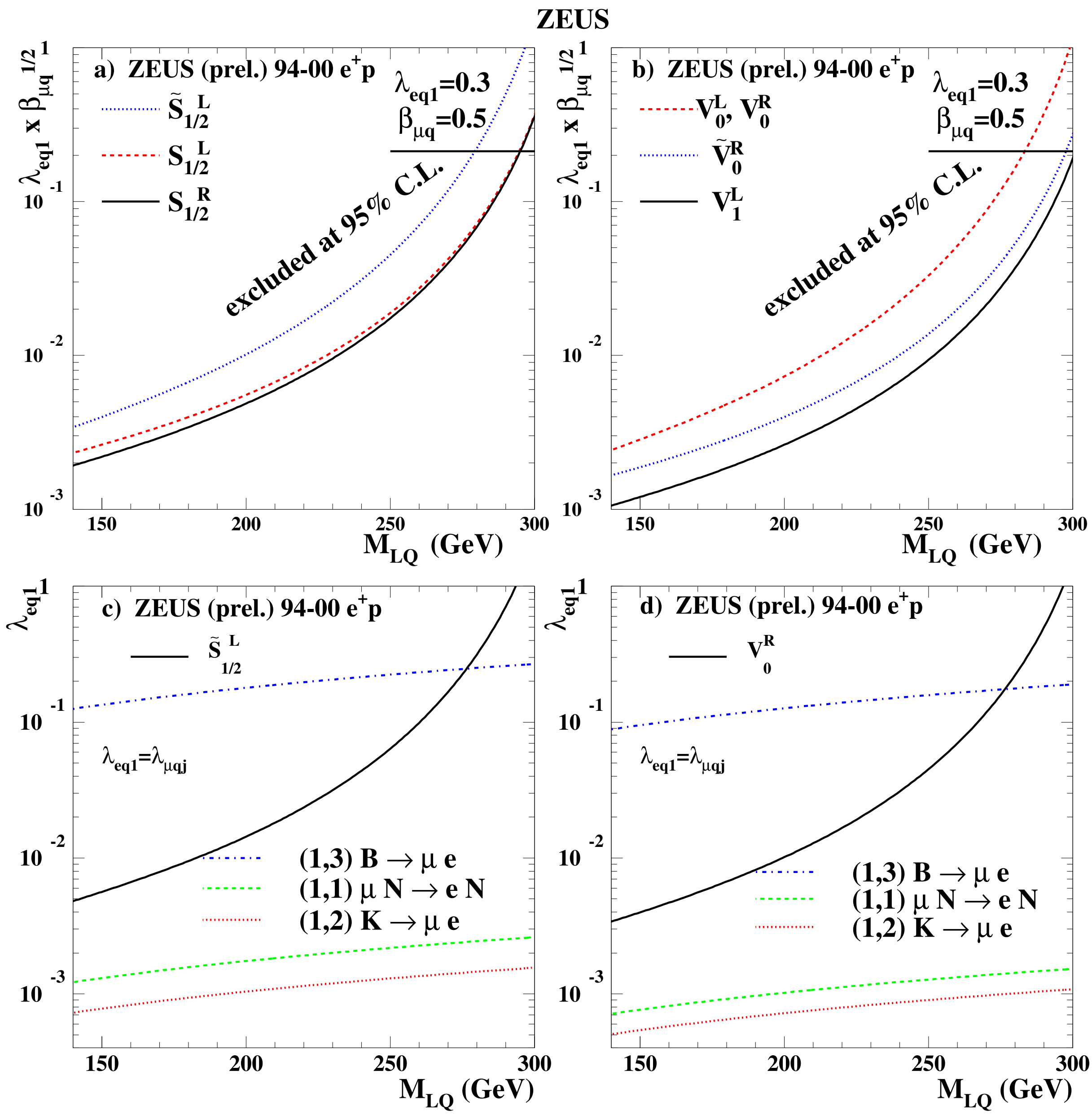

Figure 4: *Upper limits on $\lambda_{eq_1}\sqrt{\beta_{\mu q}}$ vs. M_{LQ} for a) scalar and b) vector LQs. The quark flavors that couple to the LQs in the initial state are shown in parentheses following the LQ species. Upper limits on λ_{eq_1} under the assumption $\beta_{\mu q} = 0.5$ are shown in c) for scalar LQs and d) for vector LQs that couple to d-type quarks. Also shown are existing limits [10, 29, 30] (dashed lines). The numbers in parentheses indicate the generations of the quarks that couple to the e and the μ, respectively. The regions above the curves are excluded at the 95% C.L.*